J Mater Sci (2010) 45:1371–1384
DOI 10.1007/s10853-009-4095-2

Study of tensile deformation behaviour of M250 grade maraging steel using acoustic emission

C. K. Mukhopadhyay · K. V. Rajkumar · T. Jayakumar · Baldev Raj

Received: 3 June 2009 / Accepted: 28 November 2009 / Published online: 18 December 2009

Abstract Tensile testing of solution annealed and thermally aged (755 K for various durations in the range of 0.25–100 h) specimens of M250 grade maraging steel has been carried out along with acoustic emission (AE) monitoring. Results have shown that strength increases and ductility decreases upon ageing up to 10 h and this has been attributed primarily to the precipitation of Ni_3Ti. Continued increase in strength up to 40 h of ageing has been attributed primarily to the precipitation of Fe_2Mo in addition to Ni_3Ti. Increase in ductility for 10–40 h of ageing has been attributed to dissolution of needle like Ni_3Ti precipitates and formation of fine spherical Fe_2Mo. Ageing beyond 40 h decreases strength and increases ductility due to the reversion of martensite to austenite and coarsening of the precipitates. The AE generated during tensile deformation depends on the ageing time. Increased occurrence of shearing of the precipitates by dislocations and increased brittleness of the matrix up to 10 h ageing increases the AE. The decrease in the AE beyond 10 h of ageing is due to the occurrence of deformation by Orowan looping, dissolution of Ni_3Ti precipitates and austenite reversion. The scanning electron microscopy (SEM) of the fracture surfaces has shown ductile fracture characterized by dimples and changes in the size and shape of the dimples with ageing time.

Introduction

M250 grade maraging steel possesses excellent combination of mechanical properties, i.e. ultra-high yield strength coupled with good fracture toughness [1]. Due to this combination of properties of M250 grade maraging steel, it is preferred as a structural material for critical applications in strategic sectors. In addition to these excellent mechanical properties, this steel also possesses certain other properties such as high strength to weight ratio, good weldability and easy machinability in the solution annealed condition. Moreover, the high dimensional stability achieved upon ageing of this steel, makes this steel an ideal choice for rocket motor casings in aerospace industries. The ageing behaviour of the maraging steels has been studied extensively where systematic changes in the microstructure of this steel are reported upon ageing at various temperatures for different durations [2–8]. The initial ageing regime is characterized by recovery of martensitic structure and hardening due to precipitation of hexagonal Ni_3Ti intermetallic phases. The formation of Ni_3Ti precipitates occurs rapidly due to the fast diffusion of titanium atoms [2, 3]. The intermediate ageing duration is characterized by precipitation of hexagonal Fe_2Mo intermetallic phase, followed by reversion of austenite from martensite. Since these two processes occurring during the intermediate ageing period affect the hardening in opposite manner, overall hardening saturates after reaching a maximum. Coarsening and dissolution of Ni_3Ti intermetallic phases also occur in this period which also influences the hardening behaviour. It has been reported that the maximum hardening of 18 wt% nickel maraging steel is due to the combined presence of Ni_3Ti and Fe_2Mo intermetallics [2].

It has been reported that M250 grade maraging steel attains the best combination of mechanical properties, i.e. high strength coupled with good fracture toughness when subjected to certain specific heat treatment schedule [1]. The heat treatment schedule corresponds to solution annealing (SA) at 1093 K for 1 h followed by ageing at

C. K. Mukhopadhyay (✉) · K. V. Rajkumar · T. Jayakumar · B. Raj
Indira Gandhi Centre for Atomic Research, Kalpakkam 603102, Tamil Nadu, India
e-mail: ckm@igcar.gov.in

755 K for 3–10 h; the process of ageing results in precipitation of hard intermetallic phases in low carbon soft martensitic matrix leading to the desired combination of mechanical properties. Hence, this ageing regime is considered to be of technological importance [4–8]. Further, ageing for longer duration leads to coarsening of intermetallic phases and reversion of martensite matrix to austenite; both of these microstructural alterations considerably affect the tensile as well as fracture properties of this steel.

Acoustic emission technique (AET) is an advanced non-destructive evaluation (NDE) tool that can be effectively utilized to study the micro-mechanistic aspects of tensile deformation and fracture behaviour of materials. Acoustic emission (AE) is defined as the class of phenomenon whereby transient elastic waves are generated by rapid release of energy from localized sources in a material like places of transient relaxation of stress and strain fields [9]. An AE sensor coupled to a sample undergoing dynamic changes detects the elastic energy emitted in the form of elastic waves and provides the information about the nature of dynamic changes taking place in the sample. AET has been used extensively to study various deformation and fracture processes occurring in different materials [10–15]. It is known from these studies that, in metals and alloys having a single phase microstructure, the generation of AE during tensile deformation is due to generation and motion of dislocations which give rise to a peak in the AE at initial strain ranges during tensile deformation and is associated with macroyielding.

AET has been used to study the influence of ageing on deformation behaviour in different materials. The AE generated during tensile deformation of an Al–Zn–Mg alloy increased substantially beyond an ageing time of 100 min for ageing at 393 K, and this has been attributed to the formation of shearable precipitates due to ageing where such precipitates favour strain localization and formation of coarse slip bands during tensile deformation [16, 17]. It was proposed that the passage of initial few dislocations shear the precipitates, forming a plane of weakness, which favours strain localization and subsequently, the passage of many dislocations occur to form a slip band [16, 17]. An increase in the height of the AE peak near yield after ageing for shorter duration in JBK-75 precipitation hardenable stainless steel, an experimental stainless steel hardened with a beryllium containing precipitate, and in Incoloy 903, was reported [10, 11]. This increase in the AE near yield has been attributed to the difficulty in the occurrence of cross slip of dislocations around precipitates and which are sheared or cut by dislocations thus forming initiation sites for the creation of dislocation avalanche [10, 11]. In alloy systems where the precipitates can be sheared by dislocations if the precipitates are not too strong, giving rise to dislocation avalanche which in turn leads to higher AE activity near the onset of plastic flow [11]. But in certain alloys such as precipitation hardening Al alloys, the precipitates are not easily sheared by dislocations, and the dislocations tend to loop around the precipitates instead of creating pile ups. In these alloys, a decrease in the AE has been observed in the aged condition as compared to solution annealed and quenched condition [11]. The influence of γ' precipitates on the AE generated during tensile deformation of a Ni base superalloy Nimonic alloy PE 16 has been studied [12, 18–20]. The presence of coherent γ' (radius up to 12 nm) precipitates in the aged specimens led to a large scale increase in the AE activity as compared to solution annealed specimen and this has been attributed to the deformation of γ' particles by shearing. Considerable reduction in the AE activity for specimens with γ' radius more than 19 nm was explained by loss of coherency of the γ' particles with increasing size leading to deformation essentially taking place by Orowan looping process [12, 18–20]. These studies have shown that the generation of many high energetic AE signals is associated with particle shearing process as compared to the Orwan looping process, in precipitation hardenable materials.

Even though several investigations have been carried out in the past to study the tensile behaviour of aged specimens in different materials using AET, no study has been reported so far on deformation behaviour of aged M250 grade maraging steel. Ageing of maraging steel produces complex variations in microstructural features; simultaneous variations occur in dislocation density, intermetallic precipitation (Ni_3Ti and Fe_2Mo) and reversion of martensite to austenite. This type of simultaneous variation in microstructural features during ageing of this steel is expected to influence NDE parameters in complex manner. The changes in microstructures in this steel due to ageing have been studied using different NDE parameters such as ultrasonic velocity [21], magnetic Barkhausen emission (MBE) rms voltage [22] and eddy current amplitude [23]. All these NDE studies were carried out to understand the microstructural evolution due to ageing, but the changes occurring in the deformation behaviour in aged material are not known. The AET, being a dynamic method, has potential to characterize the changes in this material during deformation. An attempt has been made in this investigation to understand the influence of various microstructural features on deformation behaviour of this steel, using AET.

Experimental

The chemical composition (wt%) of the M250 grade maraging steel used in this study is as follows: 17.89 Ni, 8.16 Co, 4.88 Mo, 0.43 Ti, 0.05 Mn, 0.05 Cr, 0.05 Si, 0.05

Cu, 0.096 Al, 0.003 C and bal. Fe. A plate of M250 maraging steel was solution annealed at 1093 K for 1 h followed by air cooling. Flat tensile specimens with gauge dimension 40 × 8 × 3 mm were fabricated from solution annealed plates and were encapsulated in quartz tubes under vacuum and aged at 755 K for different durations of 0.25, 3, 10, 40 and 100 h, followed by water quenching. The microstructural characterization of the steel in the solution annealed and aged conditions were done by transmission electron microscopy (TEM) and X-ray diffraction (XRD) techniques. The experimental details of the TEM and XRD investigations are given elsewhere [21].

Tensile tests were conducted at room temperature on specimens in the solution annealed as well as in the aged conditions at a nominal strain rate of 2.1×10^{-4} s^{-1} using Instron tensile testing machine. The AE signals generated during tensile testing of all the specimens were recorded by using a sensor with 150 kHz resonant frequency with suitable pre-amplifier (gain 60 dB) and band pass filter (100–300 kHz). The filter used allows signals to be recorded within the frequency band 100–300 kHz and discriminates signals outside this frequency band. The sensor was mounted on the upper pull rod of the tensile testing machine using vacuum grease as couplant. This part of the pull rod is stationary. Thus, the pull rod where the AE sensor is mounted does not disturb the AE measurement. On the other hand, it eliminates any variation in AE signals arising out of the sensor mounting from specimen to specimen if the sensor is directly mounted on the specimen. The AE signals generated during tensile testing of all the specimens were recorded using Spartan 2000 Acoustic Emission system of M/s. Physical Acoustic Corporation, USA. A total gain of 90 dB and a threshold of 43 dB were used. Figure 1 shows the schematic of the experimental arrangement for the AE signal recoding during the tensile testing. The gain and threshold were so selected that no external noise was recorded during the experiment. This was verified by repeatedly loading and unloading a dummy specimen to more than 1.5 times the maximum load expected to be taken by any of the specimens used in the present study. After the first cycle of loading, no emission was generated during the subsequent cycles. This indicated that the AE signals were not recorded either from the machine or from the external noise. Different parameters of the AE signal viz., root mean square (RMS) voltage, counts and peak amplitude of the AE hits were recorded during the tests and were used for analyzing the results.

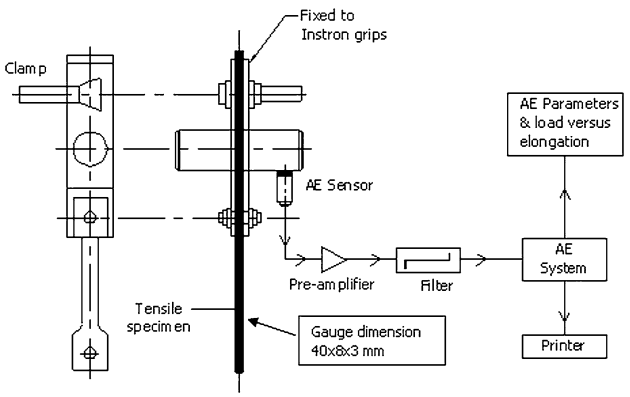

Fig. 1 Schematic of the experimental setup

The fracture surfaces of the solution annealed and different aged specimens were examined under a scanning electron microscope (SEM). For this, small samples were cut from the fracture regions of the tensile tested specimens. The energy-dispersive X-ray analyses (EDAX) of the matrix and the precipitates were also carried out.

Results and discussion

Microstructural investigations

Figure 2a shows the bright field (BF) image of the solution annealed specimen obtained by TEM which consists of lath martensite with a high dislocation density. The selected area diffraction (SAD) pattern obtained from the matrix using [110] zone axis is shown in Fig. 2b. The SAD pattern consists of reflections from the matrix only. Figure 3a, b shows the BF image of the specimen aged for 3 h and corresponding SAD pattern obtained from the matrix using [517] zone axis. It can be clearly seen from the BF image (Fig. 3a) that ageing for 3 h decreases the dislocation density and promotes the formation of very fine needle/rod shaped precipitates. The SAD pattern (Fig. 3b) shows the superlattice reflections corresponding to the Ni_3Ti precipitates. A $(0001)\eta//\{011\}_M$, $(11\bar{2}0)\eta//\langle 1\bar{1}1\rangle_M$ orientation relationship has been observed between the Ni_3Ti precipitates (η) and the matrix, as reported in the earlier investigations also [2, 24]. But for specimens aged for shorter durations, i.e. up to 1 h, the superlattice reflections corresponding to the precipitates could not be observed because of fineness of the precipitates. This is in agreement with that reported by Vasudevan et al. [2]. The BF image of the specimen aged for 30 h (Fig. 4a) exhibited the presence of larger amount of precipitates in the matrix and dark patchy reverted austenite at the lath boundaries. The SAD pattern obtained from the matrix using [317] zone axis (Fig. 4b) revealed the presence of two different types of precipitates, which are identified as Ni_3Ti and Fe_2Mo. The superlattice reflections corresponding to [317] zone axis in presence of Ni_3Ti and Fe_2Mo precipitates have been indexed. A $(0001)_{Fe_2Mo}//\{011\}_M$, $\langle\bar{2}110\rangle_{Fe_2Mo}//\langle 110\rangle_M$ orientation relationship has been observed between the Fe_2Mo

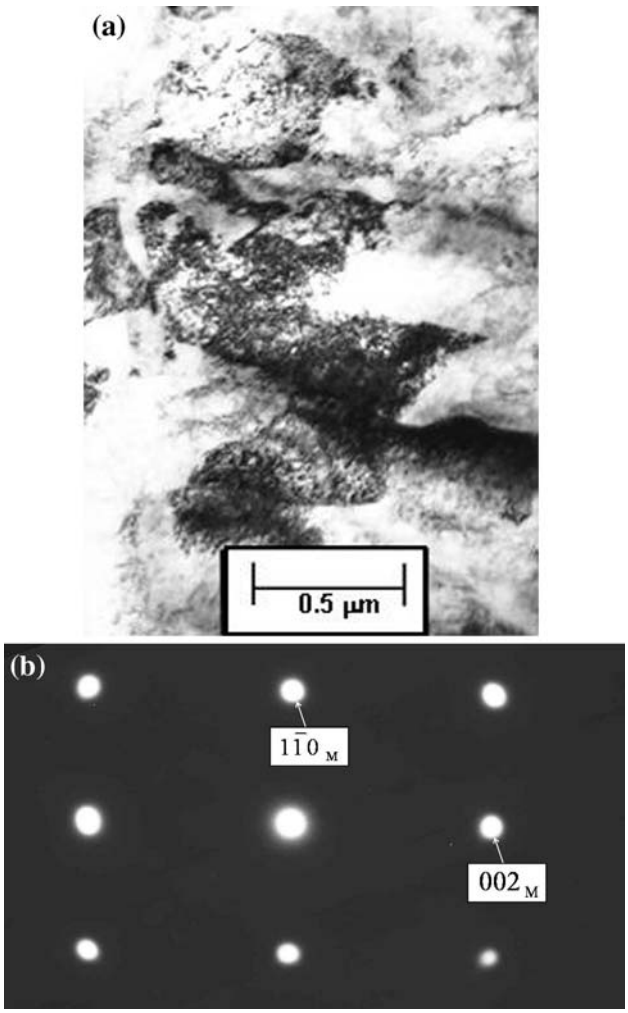

Fig. 2 **a** Bright field image (showing high dislocation density) and **b** selected area diffraction pattern taken from matrix using [110] zone axis of specimen solution annealed at 1093 K for 1 h followed by air cooling

precipitates and the matrix, which is in agreement with the earlier investigation [24].

Ageing for longer durations up to 100 h led to the increase in continuous network of patchy austenite (marked as (A) in Fig. 5a) along the martensitic lath, and coarsening of Ni_3Ti (marked as (B) in Fig. 5a) and Fe_2Mo (globular precipitates marked as (C) in Fig. 5a) precipitates. The SAD pattern (Fig. 5b) obtained from the matrix using [317] zone axis shows the presence of both Ni_3Ti and Fe_2Mo precipitates. Figure 5c shows the SAD pattern obtained using [001] zone axis of martensitic matrix from the region having reverted austenite. It shows superlattice reflections corresponding to intermetallic precipitates along with reflections from austenite phase. Various microstructural observations made in this study are in accordance with those reported in the literature [2].

X-ray diffraction technique was used to study the reversion of austenite due to ageing. During isothermal ageing at 755 K, within the experimental limit of X-ray diffraction technique, austenite could not be detected even up to 40 h of ageing. Ageing further up to 100 h resulted in increase in the volume fraction of austenite to 30%.

Tensile deformation studies

The variations of 0.2% offset yield strength and ultimate tensile strength of the selected steel upon isothermal ageing (755 K) are shown in Fig. 6. The strength was found to be minimum in SA condition. Upon ageing, the strength continued to increase to reach a maximum and decreased afterwards. The minimum in yield strength (920 MPa) is attributed to the absence of strengthening precipitates in martensitic matrix in solution annealed condition (Fig. 2a). The increase in the strength with ageing up to 40 h is attributed to the increase in the amount of strengthening precipitates (Ni_3Ti and Fe_2Mo) formed during ageing. The increase in the strength observed initially (up to 3 h) is due to the precipitation of Ni_3Ti. Further increase in strength up to 40 h is due to the precipitation of Fe_2Mo in addition to Ni_3Ti. The decrease in the strength upon ageing for longer durations (beyond 40 h) is primarily due to austenite reversion supplemented by coarsening of the precipitates due to overageing. Though TEM studies revealed the initiation of reversion of austenite at 30 h itself, decrease in the strength is observed only beyond 40 h (Fig. 6). This is attributed to the continuous precipitation of Fe_2Mo, which tends to increase the strength even beyond 30 h and takes place simultaneously along with austenite reversion. Hence, the overall decrease in the strength due to the formation of austenite can be observed only when the decrease in strength due to austenite reversion is more than the increase in strength due to continued precipitation of Fe_2Mo.

The variations in uniform elongation and total elongation with ageing time are also shown in Fig. 6. Both uniform and total elongation values vary similarly with the ageing time. The magnitude of elongation initially decreases, reaches a minimum at 10 h and then increases again upon further ageing. The observed reduction in the elongation with the associated increase in the strength up to 10 h is in line with the expected tensile behaviour for precipitation strengthened alloys. The decrease in the elongation up to 10 h is attributed to the formation of needle like Ni_3Ti precipitates. Since, these Ni_3Ti precipitates (observed at lower ageing time up to 10 h) cause stress peaks at the tips of the needles and favour nucleation and development of microcracks during deformation, thereby leading to considerable reduction in the elongation up to 10 h. Development of microcracks during deformation has been confirmed by SEM observation of fracture surfaces. However, beyond 10 h, the increase in the strength is also expected to decrease the elongation. On the contrary, the elongation is

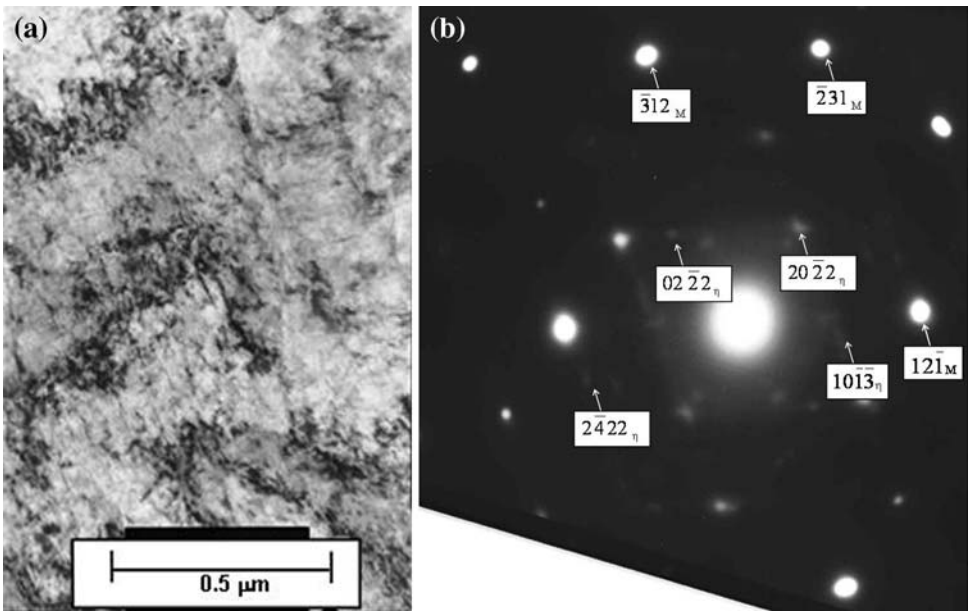

Fig. 3 **a** Bright field image of specimen thermally aged at 755 K for 3 h followed by water quenching and **b** corresponding selected area diffraction pattern taken from matrix using [517] zone axis showing superlattice reflections corresponding to $Ni_3(Ti, Mo)$ intermetallic precipitates. (Orientation relationship: $(0001)\eta//\{011\}_M$, $(11\bar{2}0)\eta//\langle 1\bar{1}1\rangle_M$; $a_M = 0.2881$ nm; $a_\eta = 0.5101$ nm and $c_\eta = 0.8307$)

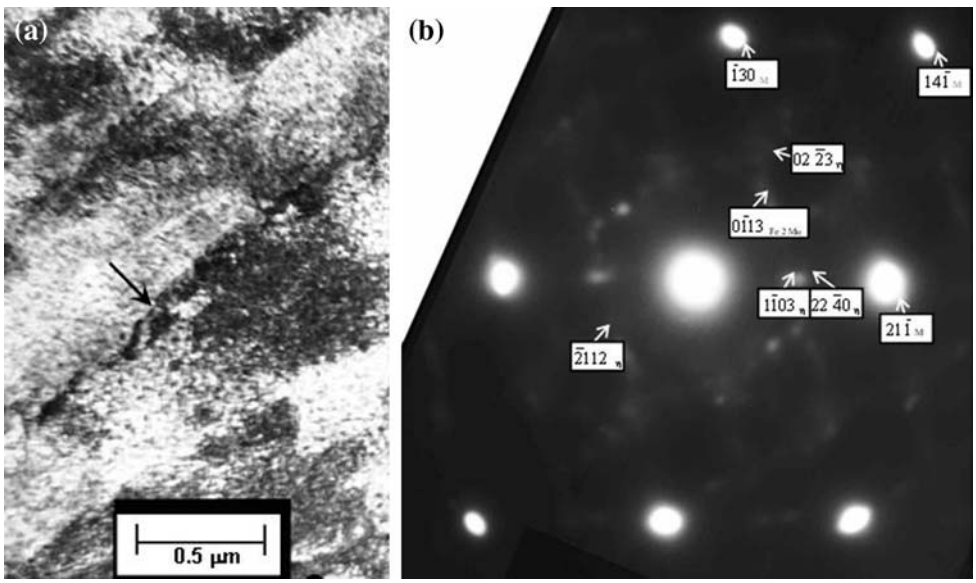

Fig. 4 **a** Bright field image of the specimen thermally aged at 755 K for 30 h followed by water quenching, showing austenite along the lath boundary (shown by *arrow*) and $Ni_3(Ti, Mo)$ and Fe_2Mo precipitates in the matrix, **b** corresponding selected area diffraction pattern obtained from matrix using [317] zone axis, showing superlattice reflections corresponding to $Ni_3(Ti, Mo)$ and Fe_2Mo intermetallic precipitates. (Orientation relationship: $(0001)_{Fe_2Mo}//\{011\}_M$, $\langle\bar{2}110\rangle_{Fe_2Mo}//\langle 110\rangle_M$; $a_M = 0.2881$ nm; $a_{Fe_2Mo} = 0.4745$ nm and $c_{Fe_2Mo} = 0.7754$)

found to increase beyond 10 h. This is attributed to dissolution of the needle type Ni_3Ti precipitates in addition to the precipitation of fine spherical (reduced stress peaks) Fe_2Mo. The combined influence of these two precipitates reduces the stress peaks leading to increase in the ductility of the matrix. The increase in both uniform and total elongations up to 100 h ageing time is again attributed to the synergistic influence of coarse spherical precipitates and increased amount of soft reverted austenite.

AE studies

The typical variations of Engineering stress, RMS voltage and AE event counts versus Engineering strain for solution annealed specimen are shown in Fig. 7a–c respectively. In Fig. 7a–c, the arrow 'A' indicates the strain corresponding to the 0.2% yield stress. In order to have a comprehensive analysis and for the ease of discussion, the variation in the total event count generated for different specimens are plotted as a function of Engineering strain in Fig. 8. Further, the AE event count generated up to yield strength (N_{YS}), up to ultimate tensile strength (N_{UTS}), and that generated between yield strength and ultimate tensile strength ($N_{UTS} - N_{YS}$) were determined. Variations of N_{YS}, N_{UTS} and ($N_{UTS} - N_{YS}$) with ageing time are shown in Fig. 9.

Comparing the obtained results (as shown in Figs. 7, 8, 9), it is observed that (a) appreciable AE is generated in the

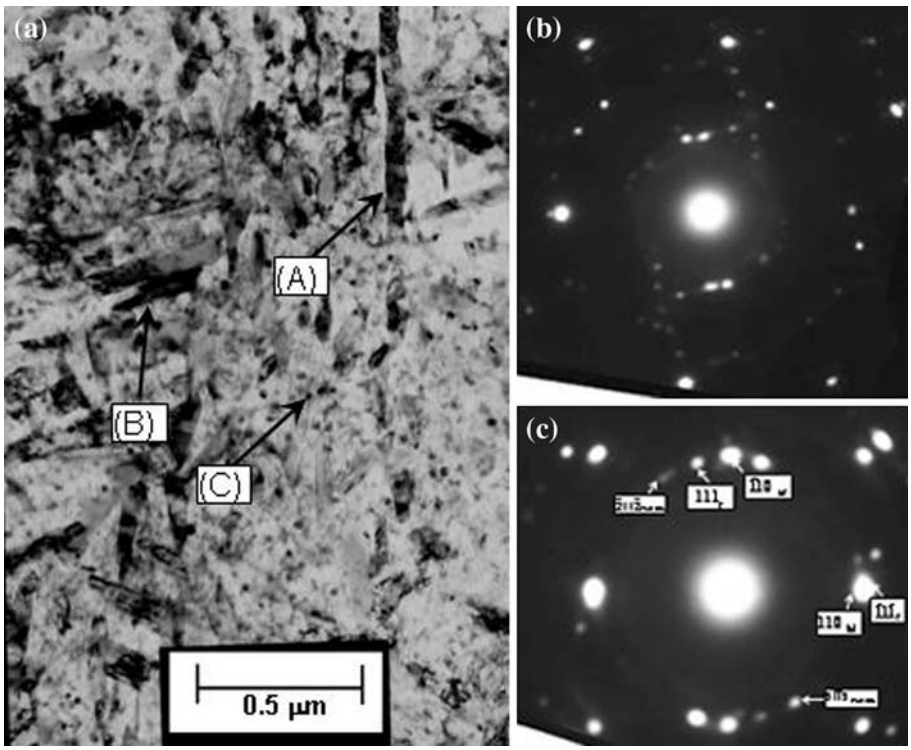

Fig. 5 **a** Bright field image of the specimen thermally aged at 755 K for 100 h followed by water quenching, showing long and patchy austenite (marked as *A*), patchy $Ni_3(Ti, Mo)$ (marked as *B*) and globular Fe_2Mo (marked as *C*), **b** corresponding selected area diffraction pattern obtained from matrix using [317] zone axis, showing superlattice reflections corresponding to $Ni_3(Ti, Mo)$ and Fe_2Mo intermetallic precipitates and **c** selected area diffraction pattern obtained from the matrix using [001] zone axis, indicating superlattice reflections corresponding to Fe_2Mo (Orientation Relationship: $(0001)_{Fe_2Mo}//(110)_M$, $[2110]_{Fe_2Mo}//[1\bar{1}0]_M$) and austenite (OR: $((\bar{1}11)_\gamma//(110)_M$ and $[121]_\gamma//[\bar{1}10]_M$)

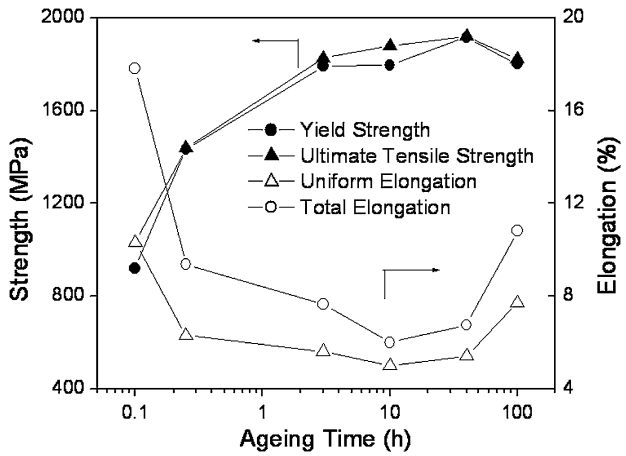

Fig. 6 Variations of strength (yield strength and ultimate tensile strength) and elongation (uniform elongation and total elongation) versus ageing time

solution annealed as well as in different aged specimens at lower strain levels up to yielding; (b) AE generated is found to be higher for the aged specimens as compared to the solution annealed specimen. Among the aged specimens, the strain at which emission starts is found to be minimum for 10 h (Fig. 8). The variation of total event count with strain shows a steep rise for the 10-h aged specimen as compared to the other specimens; (c) event count generated up to both yielding and ultimate tensile strength increases with ageing time, reaching a maximum at 10 h of ageing, but beyond that, AE generated up to both yielding and ultimate tensile strength decreases. This is similar to the variation in strength with ageing time (Fig. 6). However, the maxima in AE event counts and strength values with ageing time are observed at different time duration, i.e. at 10 and 40 h, respectively; and (d) AE generated between YS and UTS is drastically reduced for all the aged specimens as compared to the solution annealed specimen (Fig. 9).

The AE generated during tensile deformation can be understood in terms of the influence of various microscopic changes occurring during tensile deformation. As the deforming microstructure determines the strength and the generated AE in a material, the changes in the strengthening behaviour can be related to the AE generation. Hence the similarities observed in the variations in the tensile properties and the AE can be generally understood using similar reasoning except for the maxima in AE and strength observed at different ageing durations.

The AE generated during tensile deformation in the solution annealed condition is attributed to the generation and motion of dislocations and their interaction with grain/lath boundaries, since microstructure in the solution annealed condition is characterized by precipitate-free lath martensite with high dislocation density (Fig. 2a). Thus, a part of the high strength of martensite arises from the effective barriers to slip provided by high dislocation density. The high density of dislocations also serves as a source of mobile dislocations during tensile deformation and martensite lath spacing is considered to be the critical

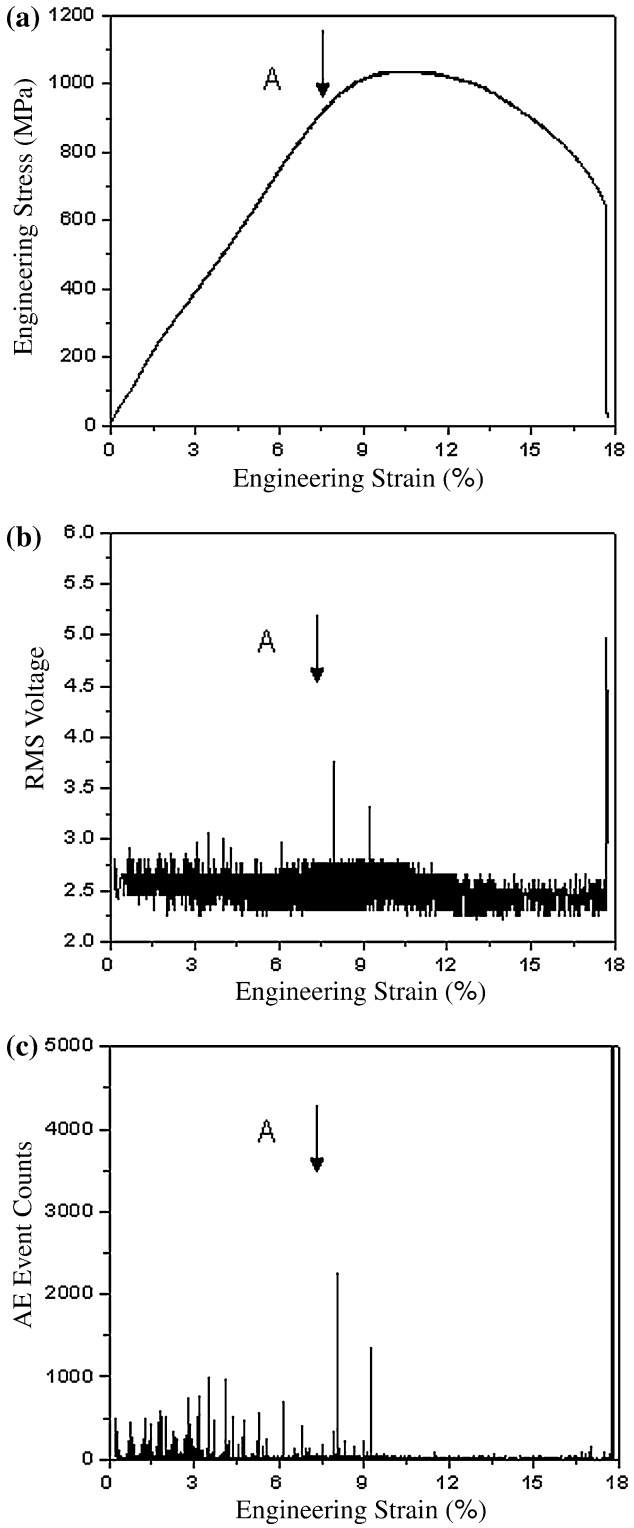

Fig. 7 Variation of **a** Engineering stress, **b** RMS voltage and **c** AE event counts versus Engineering strain plots for solution annealed specimen

slip limiting dimension [25]. As compared to the aged specimens, numerous martensite lath boundaries present in the solution annealed specimen thus limit the maximum

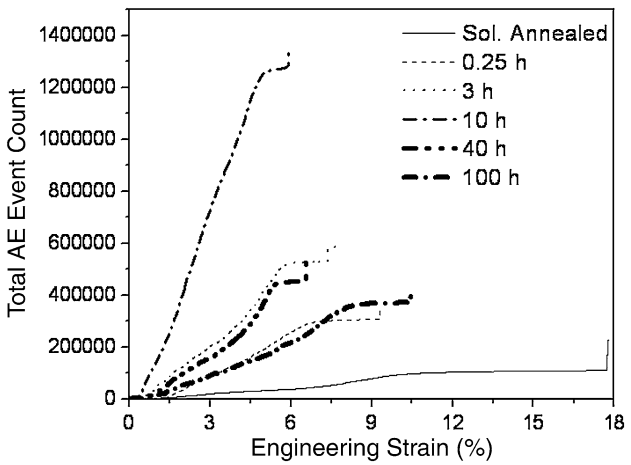

Fig. 8 Variation of total AE event count of the AE signal versus Engineering strain for the solution annealed specimens and specimens with different ageing time

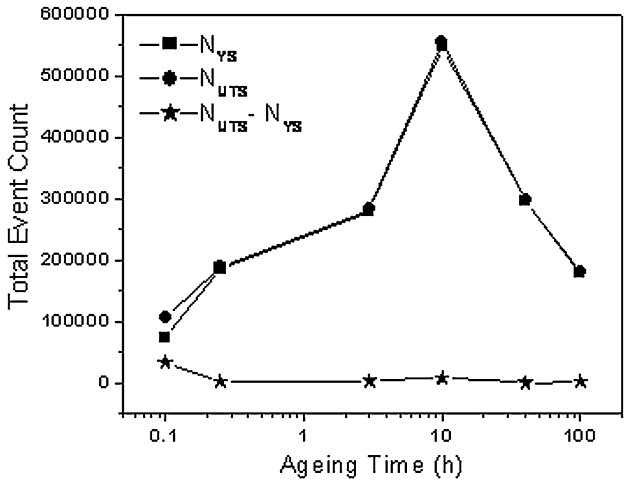

Fig. 9 Variation of event count generated up to yield strength (N_{YS}), up to ultimate tensile strength (N_{UTS}) and between YS and UTS ($N_{UTS} - N_{YS}$), as a function of ageing time

slip distance for moving dislocations. Since the AE generated by dislocation movement is governed by product of the glide distance of the dislocations and dislocation velocity, reduction in both the glide distance and dislocation velocity in the solution annealed condition reduces the AE generation in the SA specimen as compared to the aged specimens. It is also reported that in maraging steels, nickel in solid solution reduces the resistance of the crystal lattice to movement of free dislocations and also reduces the energy of interaction of dislocations with interstitial atoms [26]. Thus, nickel facilitates not only the relaxation processes by microscopic deformation, but also generation of dislocations in boundaries of former austenite grains and martensite crystals. The generation of dislocations provides increased resistance to brittle fracture by facilitating the

spread of plastic deformation from one grain to another (crystal). Since brittle fracture is associated with more AE, the observed lower AE up to yielding in the solution annealed condition as compared to the aged conditions is also attributed to the increased resistance of matrix to the brittle fracture. The high elongation (Fig. 6) for SA condition supports increased deformation. The AE activity reduces during post-yield deformation as compared to that up to yielding. This is due to the decrease in the glide distance of the moving dislocations and reduced dislocation activity. The higher AE generated during post-yield deformation in the solution annealed specimen compared to the aged specimens is attributed to the higher amount of plastic deformation exhibited by the solution annealed specimen (Fig. 6).

The AE generated in the aged specimens is higher than the solution annealed specimen and increases with ageing time. This is attributed to the synergistic influence of (i) dislocation activity, (ii) presence of intermetallic particles and (iii) improvisement of Ni in solid solution on deformation behaviour. The continuous increase in the strength (Fig. 6) and the AE generated (Fig. 9) by ageing up to 10 h can be attributed to the continuous increase in the stress required to shear the Ni_3Ti precipitates. The ageing of this steel up to 10 h is characterized by a continuous reduction of vacancies and dislocations due to annihilation, precipitation of Ni_3Ti intermetallics (Fig. 3) and associated impoverishment of nickel in solid solution. The ageing up to 10 h leads to the formation of coherent precipitates initially (up to 3 h), which upon further ageing increases the size of the precipitates leading to partial loss of coherency (semi-coherent). This is due to the formation of hcp Ni_3Ti precipitates with a lattice mismatch of 2.22% between close packed planes of Ni_3Ti and the martensite matrix [27]. Due to this, precipitates having greater than 10 nm size become incoherent with the matrix [5]. The mismatch between the precipitates and the matrix interface is accommodated by the formation of interfacial dislocations [5]. The increase in the AE with increasing ageing time up to 10 h is thus attributed to the shearing of both coherent and semi-coherent Ni_3Ti precipitates, which result in strain localization and formation of slip bands in the matrix. Once the precipitates are sheared by dislocations, the cross sections of the precipitates are reduced, decreasing the stress acting on the slip plane. This leads to the weakening of the particles and concentration of dislocations on the particular slip plane, thus creating slip bands in the matrix. The number of dislocations (N) formed in a slip band due to particle shearing below the critical particle size is given by [28]:

$$N = Kf^{1/2}r^{1/2}L \tag{1}$$

where K is constant, f is the volume fraction of particles, r is the radius of the particle and L is the length of the dislocation pile up. Equation 1 indicates that the intensity of slip expressed by number of dislocations increases with increasing volume fraction and radius of the particles and length of the dislocation pile up. With increasing ageing time up to 10 h, although L decreases due to increase in the volume fraction and radius of the particles, the combined effect of these two factors increases the generation of dislocations. As indicated earlier, the alloy systems in which such dislocation–precipitation interactions by shearing are reported, include Al–Zn–Mg alloy, JBK-75 precipitation hardenable stainless steel, Incoloy 903 and Nimonic PE-16 Superalloy [10–12, 16–20]. The results of higher AE for ageing time up to 10 h in M250 maraging steel used in the present investigation are in agreement with the above mentioned studies, where higher AE in the aged specimens has been attributed to the presence of shearable precipitates and such precipitates favour strain localization, formation of dislocation avalanche and coarse slip bands. The presence of intermetallic precipitates has been confirmed by SEM observation of fracture surfaces. The fractograph of the 0.25-h aged specimen along with the EDAX result of one particle obtained are depicted in Fig. 10a, b. This shows that the fracture surface is ductile dimple type and precipitate formed after 0.25 h of ageing is rich in titanium. The EDAX results of the matrix and one particle for 3 h aged specimen are shown in Fig. 11a, b, respectively. This shows that both matrix and the particle after 3 h ageing are rich in Fe.

The generation of higher AE at lower strain levels in the aged specimens than in the solution annealed specimen of M250 maraging steel is therefore associated with major strengthening by ageing in a precipitation hardenable material and this arises from the irreversible energy change occurring during interactions between the dislocations and the particles, as the dislocations shear through the particles [29]. The interactions of dislocations with particles due to chemical, order, coherence, stacking faults and modulus strengthening occur when the deformation takes place by particle shearing, resulting in the increase in the flow stress and the release of acoustic energy. The occurrence of precipitation hardening by particle shearing enhances the flow stress of the aged specimens compared to the solution annealed specimen and the increase in the flow stress ($\Delta\sigma$) is given by the following equation [19, 29]:

$$\Delta\sigma = K' r^a f^b (\Delta E)^c \tag{2}$$

where K' is the material constant, r is the radius of the particle, f is the volume fraction of particles, ΔE is the irreversible energy change associated with various dislocation-particle interactions, and a, b and c are constants. In Eq. 2, the values of a and b were reported to be less than 1 and the value of c as greater than 1 [29]. It is thus understood from Eq. 2 that the magnitude of ΔE will have more

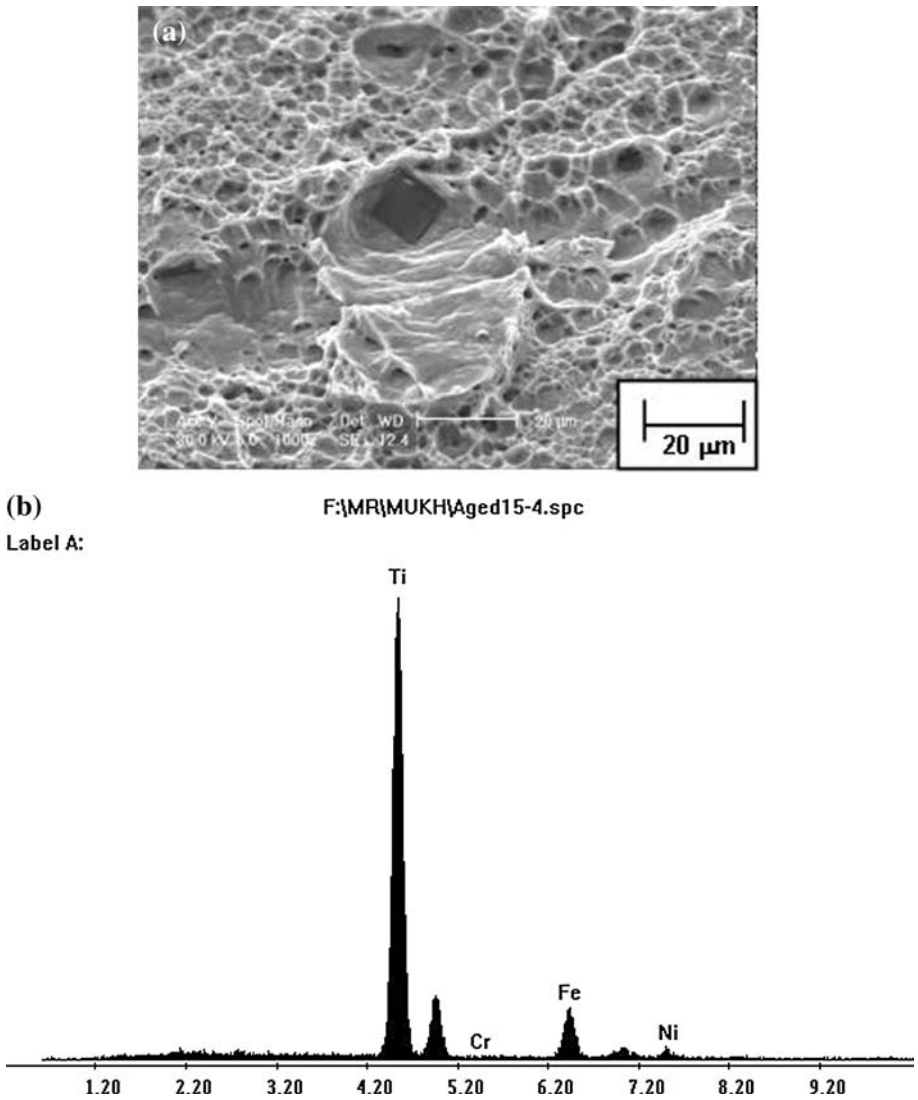

Fig. 10 **a** SEM fractographs of 0.25 h aged specimen alongwith **b** EDAX results

effect for the increase in flow stress as compared to *r* or *f*. Thus, the occurrence of particle shearing in aged specimens should result in higher energy release through different dislocation–particle interactions. The impoverishment of nickel in solid solution also takes place in this regime. The impoverishment of the solid solution in nickel due to ageing impairs the properties of the matrix by promoting the tendency of crack nucleation. This not only increases the tendency for brittle fracture of the specimens aged up to 10 h, as evidenced by reduction in the elongation, but also the generation of AE. Hence the increase in the AE observed up to 10 h can be attributed to the net manifestation of the AE generated due to precipitate shearing by dislocations and by increased tendency to brittle fracture of the matrix.

The AE generated in the aged specimens increases up to 10 h and decreases beyond that. Ageing for 10–40 h leads to: (a) increase in the size of the Ni_3Ti and partial loss of coherency, (b) formation of coherent Fe_2Mo precipitates, (c) dissolution of Ni_3Ti precipitates and (d) initiation of reversion of martensite to austenite. The ageing for durations greater than 10 h results in precipitate size of Ni_3Ti greater than 10 nm, which is evident from the BF image corresponding to 30 h of ageing (Fig. 4a). Because of the presence of such incoherent precipitates in the matrix, the precipitates are not sheared by dislocations and the propagation of dislocations takes place by looping around the precipitates. The occurrence of deformation by looping around the precipitates, i.e. Orowan looping is known to occur in precipitation hardenable materials with presence of large precipitates [11]. The decrease in the AE generated beyond 10 h of ageing time is thus attributed to the occurrence of the part of the deformation by Orowan looping. This occurs in addition to the deformation taking place by shearing of semi-coherent Ni_3Ti and coherent Fe_2Mo precipitates. The net effect is the reduced AE generation for specimens aged in this regime.

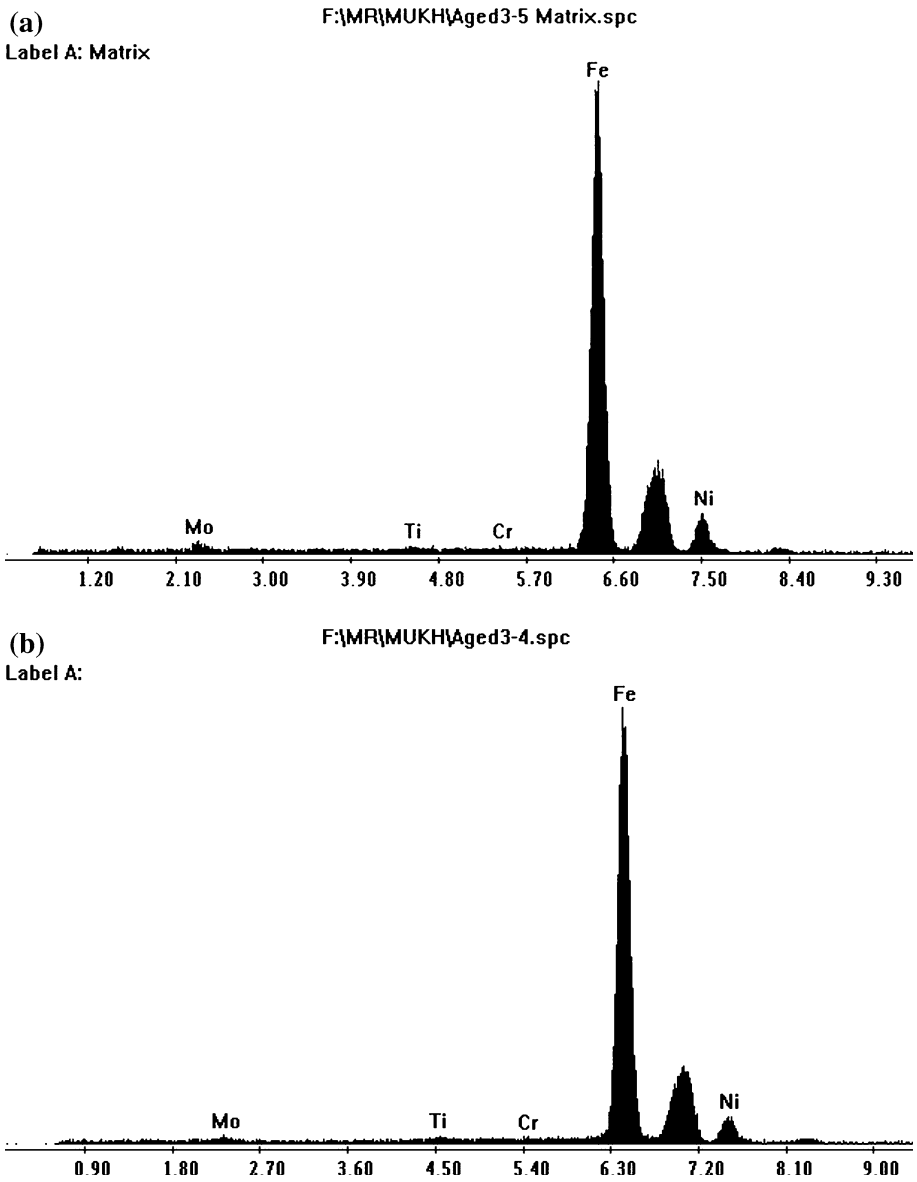

Fig. 11 EDAX results of **a** matrix and **b** particle shown for 3 h aged specimen

The maximum in the AE generated at 10 h does not coincide with the maximum in the strength values occurring at 40 h. The ageing for 40 h leads to increase in the precipitation of Fe_2Mo along with dissolution of Ni_3Ti, and hence the maximum in the strength at 40 h is attributed to the maximum volume fraction of combined precipitates (Ni_3Ti and Fe_2Mo). The interaction of dislocations with these complex microstructures increases the stress required for dislocation looping (in the case of in-coherent Ni_3Ti) as well as for particle shearing (in the case of coherent Fe_2Mo) leading to increase in the strength from 10 h to 40 h. The shearing of the coherent Fe_2Mo precipitates is expected to generate energetic AE but coarsening and dissolution of Ni_3Ti precipitates, enrichment of nickel and initiation of austenite reversion in the matrix, all lead to reduction in the AE generation beyond 10 h. On prolonged ageing, the metastable precipitates dissolve resulting in local enrichment of nickel at preferred sites where austenite reversion is initiated [30]. During tensile deformation of the specimens with reverted austenite, the load is concentrated on soft austenite as compared to martensite leading to large elongation. The easy flow of dislocations in these specimens lowers the AE generation. Hence the net manifestation is found to have an overall decrease in AE for the 40 h aged specimen as compared to 10 h. It is reported that deformation of austenite generates weak AE signals [12].

The ageing beyond 40 h decreases the AE generation. The ageing beyond 40 h is characterized by (a) precipitation and coarsening of Fe_2Mo leading to incoherency; (b) coarsening and increased dissolution of incoherent Ni_3Ti;

and (c) increase in the volume fraction of reverted austenite. Upon ageing for more than 40 h, incoherent Fe_2Mo precipitates occur at longer durations (Fig. 5). The mismatch between the martensitic matrix and the Fe_2Mo precipitates is very high (4.9%) as compared to Ni_3Ti (2.22%) precipitates [27]. The loss of coherency of the precipitates is associated with a critical particle radius, $r > \mathbf{b}/\delta$, where **b** is Burger's vector and δ is lattice mismatch [31]. Thus, the precipitate size required to form incoherency is smaller in the case of Fe_2Mo compared to Ni_3Ti. As non-coherent precipitates of Ni_3Ti and Fe_2Mo are present in the specimens beyond 40 h of ageing (Fig. 5a), deformation of the 100 h aged specimen takes place by Orowan looping. The observed decrease in the strength beyond 40 h of ageing time is thus due to increase in the size and the spacing of the particles and can be understood using the concept of Orowan looping. The increase in the yield strength due to Orowan looping ($\Delta\sigma_{Or}$) is given by [32]:

$$\Delta\sigma_{Or} = K'' \frac{\ln\left(\frac{2r}{b}\right)}{\lambda} \tag{3}$$

where K'' is constant and λ is inter-precipitate distance. It can be understood from Eq. 3 that for the overaged specimens, while increasing λ decreases $\Delta\sigma_{Or}$, increasing r increases the $\Delta\sigma_{Or}$ resulting in overall increase in the strength of 40 and 100 h aged specimens as compared to solution annealed specimen. With longer ageing time, precipitates grow larger and stronger and are not sheared and these precipitates restrict the glide distance of any dislocation avalanches. But the loss of strength beyond 40 h of ageing is also associated with the lower strength of soft reverted austenite formed. Since the AE generation in this regime is primarily determined by looping of dislocations around the non-coherent precipitates and other phenomena such as austenite reversion and dissolution of precipitates, the net manifestation is the reduction in AE. When the deformation takes place by the Orowan looping process, interactions due to chemical, order, coherence, stacking fault and modulus strengthening between dislocations and particles do not occur and hence no increase in the acoustic energy could be observed. In addition to the occurrence of deformation by dislocation looping for the specimens aged beyond 40 h, precipitation of Fe_2Mo would result in depletion of Fe from the martensite matrix, thus raising the relative Ni content of the martensite. The Ni content of matrix is also increased by the dissolution of the Ni_3Ti precipitates. Both these mechanisms lead to increase in the volume fraction of soft reverted austenite in the matrix leading to further reduction in the AE generation.

The AE signals generated during the tensile deformation of the maraging steel specimens have also been analyzed using the cumulative peak amplitude distribution of the AE events (Fig. 12). It is seen that, for the solution annealed specimen where there are no precipitates, events up to 76 dB peak amplitude are generated. But in the aged specimens where precipitates are present, events of higher peak amplitudes (>76 dB) are also generated. The number of higher peak amplitude events are more for 10 h aged specimen as compared to other specimens. The maximum number of events with higher peak amplitudes generated for the 10 h ageing time is thus attributed to the energetic emission associated with dislocation movement by shearing and brittle matrix fracture. The decrease in the number of higher peak amplitude events for the specimens aged for 40 and 100 h is attributed to the deformation taking place by dislocation looping, preferential deformation of soft austenite, and decrease in the tendency for brittle matrix failure.

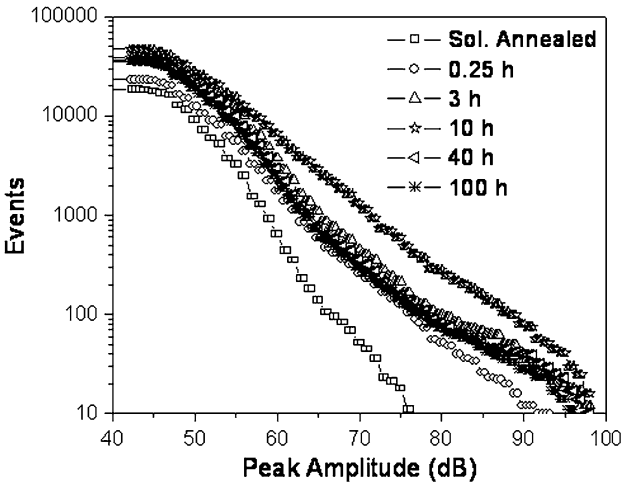

Fig. 12 Cumulative peak amplitude distribution of events for the solution annealed specimen and specimens with different ageing time

SEM studies

Observation of fracture surfaces of solution annealed and different aged specimens using SEM has been carried out. The fractographs taken are shown in Fig. 13a–f for the solution annealed specimen (Fig. 13a) and the specimens with ageing time of 0.25 h (Fig. 13b), 3 h (Fig. 13c), 10 h (Fig. 13d), 40 h (Fig. 13e) and 100 h (Fig. 13f). The fractographs of different specimens indicate ductile dimple type fracture. For the specimens aged up to 40 h, dimples are smaller in size and shallow compared to large sized and deep dimples for the solution annealed condition. The number of small and shallow dimples is maximum for the 10 h aged specimen. For ageing beyond 10 h, dimples again become large and deep. The size of dimples in the fracture surface is governed by number and distribution of microvoids that are nucleated. When the sites of void

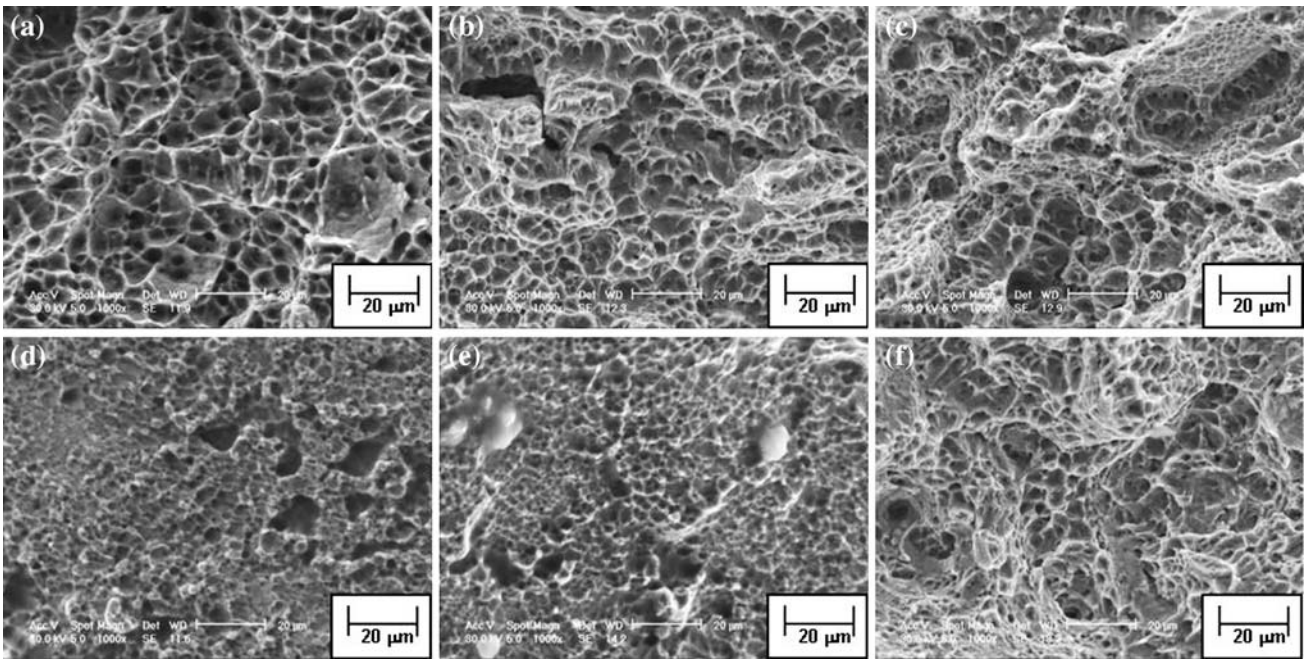

Fig. 13 SEM fractographs of specimens with different ageing time: **a** solution annealed, **b** 0.25 h, **c** 3 h, **d** 10 h, **e** 40 h and **f** 100 h

nucleation are a few and widely spaced, the microvoids grow to large size before coalescence giving rise to the appearance of a fracture surface containing large dimples. Small dimples are formed when many void nucleating sites are activated and adjacent microvoids coalescence before they can grow to a large size. On the other hand, dimple shape is governed by the state of stress in the material as the microvoids form and coalesce. The small dimples observed up to 40 h ageing could possibly be the result of localized deformation between the precipitates where the growth of voids from the adjacent particles limits the final dimple size to a value nearly equal to the average inter-particle spacing. Thus, the growth of voids is restricted to small size. The occurrence of deformation by particle shearing is expected to give rise to the localization of deformation near the particles and result in fracture appearance involving small and shallow dimples [33]. This is confirmed by dimples of mixed types for specimens aged for 0.25, 3 and 10 h and the smallest and shallowest dimples for the 10 h. This is in agreement with the fracture characteristics in precipitation hardening alloys that microvoids are nucleated at the sites of the precipitates due to (i) incompatible stress–strain behaviour of the matrix and the precipitates, (ii) localized deformation in the soft precipitate-free zone associated with grain boundary precipitates and (iii) shearing of precipitates by dislocations, giving rise to inhomogeneous planar slip bands inside the grains that may terminate at grain boundaries and, subsequently, apply large stress concentrations to augment grain boundary fracture [34]. This is also in agreement with the observation of shallow dimples in the aged specimens with increasing ageing time of maraging steel and this was attributed to the decrease in ductility with increasing hardening from underageing to peak ageing condition [35]. It is reported that the formation of very fine dimples in the peak aged condition in 18 Ni maraging steel is attributed to the fracture of very fine intercrystalline precipitates [36]. It is also reported that the formation of shallow dimples in the aged specimens could be the result of joining of the microvoids by shear along the slip bands [37]. The formation of microcracks in the aged specimen is evident from the fracture surface of the specimen aged for 0.25 h (Fig. 13b). The fracture surface of the specimens aged for 10 and 40 h also show holes that could have formed by pulling out of the precipitates. For the 100 h aged specimen, majority of the dimples appear to be large and deep. This is attributed to the occurrence of deformation over a larger volume of the material where deformation occurs mainly by Orowan looping and also by bulk deformation of the austenite. Since the deformation is not restricted in the regions between the particles and spreads over a relatively larger volume of the material, dimples increase in size and become deep. Under such conditions, voids initiating at particular particles can grow to a uniform size considerably in excess of the average spacing of the particles without the interference of the adjacent particles. Formation of large and deep dimples in the overaged specimens of maraging steel is reported [35].

The study has clearly brought about the various micro-mechanistic aspects that are responsible for the observed variations in the AE behaviour in solution annealed and various specimens of aged M250 maraging steel with different microstructural features and micro-mechanisms of tensile deformation and fracture.

Conclusion

The influence of microstructural changes on tensile deformation and associated AE behaviour in M250 grade maraging steel has been studied. The increase in the strength and the corresponding decrease in the elongation up to 10 h ageing have been primarily attributed to the intermetallic precipitation of Ni_3Ti. Further increase in the strength up to 40 h has been attributed primarily to the precipitation of Fe_2Mo in addition to Ni_3Ti. Ductility for 10–40 h ageing increases due to dissolution of needle like Ni_3Ti precipitates and formation of fine spherical Fe_2Mo. Beyond 40 h, the decrease in the strength and the increase in the ductility are attributed to the reversion of martensite to austenite and coarsening of the precipitates. The AE generated during tensile deformation generally exhibits variation similar to the strength upon ageing, where, AE increases with ageing time up to 10 h and decreases thereafter. The increase in the AE generation up to 10 h has been attributed to the increase in the shearing of precipitates by dislocations and increase in the brittleness of the matrix. Beyond 10 h, the decrease in the AE generation is due to the occurrence of dislocation movement by looping, initiation of dissolution of Ni_3Ti precipitates and austenite reversion. The maximum number of hits with higher peak amplitudes generated for the 10 h ageing time is due to energetic emission associated with dislocation movement by shearing and brittle matrix fracture. The decrease in the number of higher peak amplitude hits for the specimens beyond 40 h of ageing has been attributed to the occurrence of deformation by dislocation looping, preferential deformation of soft austenite and decrease in the tendency for brittle matrix failure. The observation of fracture surface has shown essentially ductile dimple fracture in all the specimens. The changes in the characteristics of the dimples to shallow and small in specimens aged up to 40 h compared to large and deep dimples in the solution annealed condition has been attributed to the fracture characteristics in precipitated hardened materials.

Acknowledgements Authors thank Dr. P. R. Vasudeva Rao, Director, Metallurgy and Materials Group, Indira Gandhi Centre for Atomic Research, Kalpakkam for encouragement and support. Authors thank Dr. B.P.C. Rao, Head, Electromagnetics, Modelling, Sensors and Imaging Section, Non Destructive Evaluation Division (NDED), IGCAR for many useful discussions. Authors also thank Dr. Anish Kumar, NDED, and Mrs. M. Radhika, Physical Metallurgy Division, IGCAR, for their help in TEM and SEM works, respectively.

References

1. Miller GP, Mitchell WI (1965) J Iron Steel Inst 203:899
2. Vasudevan VK, Kim SJ, Wayman CM (1990) Metall Trans A21:2655
3. Sha W, Cerezo A, Smith GDW (1993) Metall Trans A24:1221
4. Decker RF, Floreen S, Wilson RK (eds) (1988) Maraging steels: recent developments and applications. TMS-AIME, Warrendale, PA, p 1
5. Viswanathan UK, Dey GK, Asundi MK (1993) Metall Trans A24:2429
6. Sha W, Cerezo A, Smith GDW (1993) Metall Trans A24:1241
7. Sha W, Cerezo A, Smith GDW (1993) Metall Trans A24:1251
8. Guo Z, Sha W, Vaumousse D (2003) Acta Mater 51:101
9. Mclntire P (1987) In: Mclntire P (ed) Nondestructive testing handbook, vol 5, 2nd edn. American Society for Nondestructive Testing, Columbus, OH
10. Heiple CR, Carpenter SH (1987) J Acoust Emiss 6:177
11. Heiple CR, Carpenter SH, Carr MJ (1981) Met Sci 15:587
12. Baldev R, Jayakumar T (1991) Acoustic emission: current practices and future directions, ASTM STP 1077. American Society for Testing and Materials, Philadelphia, PA, p 218
13. Mukhopadhyay CK, Ray KK, Jayakumar T, Baldev R (1998) Mater Sci Eng A255:98
14. Frantisek C, Klose Frank B, Hanno D, Jindrich S, Hartmut N, Pavel L (2007) Mater Sci Eng A462:53
15. Thiebaud R, Patrik D, Frantisek C, Jerome W, Francois L (2006) Mater Sci Eng A424:190
16. Rusbridge KL, Scruby CB, Wadley HNG (1983) Mater Sci Eng A59:151
17. Scruby CB, Wadley HNG, Rusbridge KL (1983) Mater Sci Eng A59:169
18. Jayakumar T, Baldev R, Bhattacharya DK, Rodriguez P, Prabhakar O (1991) Scripta Metall Mater 25:2733
19. Jayakumar T, Baldev R, Bhattacharya DK, Rodriguez P, Prabhakar O (1992) Mater Sci Eng A150:51
20. Jayakumar T, Baldev R, Bhattacharya DK, Rodriguez P, Prabhakar O (1993) J Acoust Emiss 11:43
21. Rajkumar KV, Anish K, Jayakumar T, Baldev R, Ray KK (2007) Metall Mater Trans A38:236
22. Rajkumar KV, Vaidyanathan S, Anish K, Jayakumar T, Baldev R, Ray KK (2007) J Magn Magn Mater 312:359
23. Rajkumar KV, Rao BPC, Sasi B, Anish K, Jayakumar T, Baldev R, Ray KK (2007) Mater Sci Eng A464:233
24. Tewari R, Mazumder S, Batra IS, Dey GK, Banerjee S (2000) Acta Mater 48:1187
25. Rack HJ (1978) Mater Sci Eng 34:263
26. Spektor YI, Sarrak VI, Engin RI (1964) Dokl Akad Nauk SSSR 155(5):1054
27. Habiby F, Siddiqui TN, Hussain H, Ul Haq A, Khan AQ (1996) J Mater Sci 31:305. doi:10.1007/BF01139144
28. Blankenship CP Jr, Hornbogen E, Starke EA Jr (1993) Mater Sci Eng A169:33
29. Nicholson RB (1971) Proceedings of conference on effect second phase particles on the mechanical properties of steel. Cox and Wyman, London, p 1
30. Rack HJ, Kalish D (1971) Metall Trans 2:3011
31. Gleiter H (1967) Acta Metall 15:1213, 1223
32. Brown LM, Ham RK (1971) In: Kelly A, Nicholson RB (eds) Strengthening methods in crystals. Amsterdam, Elsevier, p 9

33. Burghard RC (1974) Metall Trans 5:2083
34. Vasudevan AK, Doherty RD (1987) Acta Metall 35:1193
35. He YI, Yang KE, Sha WEI (2005) Metall Mater Trans A36:2273
36. Viswanathan UK, Dey GK, Sethumadhavan V (2005) Mater Sci Eng A398:367
37. May LE (1977) In: McCall JK. French PM (eds) Metallography in failure analysis. ASM